Hydrothermal synthesis of $LnMnO_3$ (Ln = Ho–Lu and Y): exploiting amphoterism in late rare-earth oxides†

Evan S. Stampler,‡[a] William C. Sheets,‡[ab] Wilfrid Prellier,[b] Tobin J. Marks[a] and Kenneth R. Poeppelmeier*[a]

Received 8th January 2009, Accepted 24th March 2009
First published as an Advance Article on the web 16th April 2009
DOI: 10.1039/b900370c

The reactivity of Mn_2O_3 and late rare-earth sesquioxides in alkaline aqueous solution affords a high-yield formation of rare-earth manganites, $LnMnO_3$ (Ln = Ho–Lu and Y). The yield of the products depends significantly on the pH, which determines the solubility of the manganese cation, and reaction temperature, which regulates the decomposition of the insoluble rare-earth trihydroxide, $Ln(OH)_3$, to the more reactive oxide hydroxide, LnO(OH). Plate- and needle-like $LnMnO_3$ crystallites of a few micrometers in size have been prepared at reaction temperatures where the rare-earth oxide hydroxide is thermodynamically stable, whereas at lower temperatures the insoluble rare-earth trihydroxide persists and no reaction is observed.

Introduction

Rare-earth manganites of composition $LnMnO_3$ have been studied for over a half-century owing to their remarkable ferroelectric, ferromagnetic, and magnetoresistive properties.[1–5] Renewed interest in these compounds stems from recent studies reporting the coexistence and possible coupling of magnetic and ferroelectric properties.[6–11] Such multiferroic materials have potential application in next-generation devices, including spin-based transistors and advanced magnetic memory storage elements. Rare-earth manganites of the formula $LnMnO_3$ prepared by classic ceramic methods at ambient pressure crystallize in one of two space groups: early rare-earth manganites (Ln = La–Dy) adopt the orthorhombic perovskite structure, space group *Pnma*, while late rare-earth (Ln = Ho–Lu), yttrium, and scandium manganites have a hexagonal structure, space group $P6_3cm$.[12] The former structure is that of a Jahn–Teller distorted perovskite, Fig. 1a,[13–15] while the latter consists of *ABCACB*… stacking of close packed oxygen layers with the 5-coordinate manganese ions occupying corner-sharing trigonal bipyramids in the (001) planes and the rare-earth cations in 7-coordinate interstices, Fig. 1b.[2,16] Introduction of small rare earth cations induces large cooperative rotations of the $MnO_{6/2}$ octahedra, which destabilize the perovskite structure and favor the hexagonal structure. The structural transition is a fluid crossover between holmium and dysprosium, and $HoMnO_3$,[17] $YMnO_3$,[18] and $DyMnO_3$[19] have been stabilized in both space groups using soft chemical methods or thin film processes. Nonetheless, all $LnMnO_3$ members can be formed in the orthorhombic structure using high pressure.[20]

While $LnMnO_3$ perovskites exhibit interesting properties such as colossal magnetoresistance and magnetic ordering,[5,21] hexagonal rare-earth manganites have been studied extensively owing to their magnetic and ferroelectric properties.[22] The ferroelectric properties of hexagonal rare-earth manganites result from a cooperative tilting of the MnO_5 bipyramids below the Curie temperature (T_C) which displaces the rare-earth ions along the *c* axis. At the same time, magnetic coupling between the spins of the close-packed Mn^{3+} cations of an (001) plane is frustrated, as indicated by the low antiferromagnetic spin-ordering temperature (T_N).[23] Recent studies of phase-pure hexagonal rare-earth manganites, such as $YMnO_3$, have reported coupling between the ferroelectric and magnetic (antiferromagnetic) orderings.[24,25] Anomalies in the dielectric constant and loss tangent near the Néel temperature of $YMnO_3$ have been reported as evidence of coupling between the ferroelectric and antiferromagnetic orders. The replacement of non-magnetic Y^{3+} with magnetic Ho^{3+} at the ferroelectrically active rare-earth cation site results in an even larger increase in the dielectric constant with the onset of manganese and holmium magnetic order.[26] Reports of magnetoelectric coupling in other hexagonal rare-earth manganites, such as $LuMnO_3$, necessitates the investigation of new synthetic routes towards members of the $LnMnO_3$ family.[27–29]

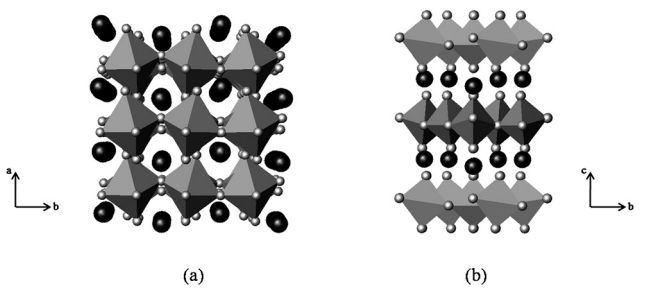

(a) (b)

Fig. 1 A schematic representation of the two $LnMnO_3$ structures. (a) The orthorhombic structure along the *c*-axis, where the gray octahedra and black spheres represent $Mn^{3+}O_6$ polyhedra and Ln^{3+}, respectively and, (b) the hexagaonal $LnMnO_3$ structure perpendicular to the *c*-axis, where the gray trigonal bipyramids and black spheres depict $Mn^{3+}O_5$ polyhedra and Ln^{3+} ions, respectively.

[a]*Department of Chemistry, Northwestern University, Evanston, IL, 60208, USA. E-mail: krp@northwestern.edu*
[b]*Laboratoire CRISMAT, CNRS UMR 6508, ENSICAEN, 6 Blvd. Maréchal Juin, F-14050 Caen Cedex, France*

† This paper is part of a *Journal of Materials Chemistry* issue in celebration of the 75th birthday of C. N. R. Rao.

‡ Authors with equal contributions.

Traditionally, samples of rare-earth manganites have been synthesized by a solid state reaction between the appropriate rare-earth sesquioxide and manganese oxide. In such reactions, a high temperature anneal (1400 °C) is necessary to eliminate the persistent Mn_3O_4 alternate phase that complicates magnetic susceptibility measurements. Recently, certain rare-earth manganites, such as $LnMn_2O_5$ (Ln = La, Pr, Nd, and Tb)[30] and $LnMnO_3$ (Ln = Sm–Ho),[31] were generated by hydrothermal methods. Members of the $LnMn_2O_5$ series were prepared by first precipitating a K-birnessite gel *via* the addition of KOH to a solution containing $KMnO_4$ and $MnCl_2$, which was then placed in an ice bath. This was followed by the addition of the respective rare-earth oxide (Ln_2O_3) and a concentrated solution of KOH (~13.4 M), the excess of which acts as mineralizer during the reaction. Upon stirring, the solutions were treated hydrothermally at 240 °C for 3 days and small single crystals were collected. Single crystals of $LnMnO_3$ (Ln = Sm–Ho) were prepared by the same procedure. The authors reported that similar reactions failed to yield the late rare-earth manganites, $LnMnO_3$ (Ln = Er–Lu), and attributed this result to the low solubility of late rare-earth trihydroxides.

Owing to the absence of reports on the hydrothermal synthesis of the hexagonal late rare-earth manganites, their interesting magnetoelectric properties, and the high molar solubility of Mn_2O_3 in aqueous media at high pH, the rare-earth manganites of composition $LnMnO_3$ (Ln = Ho–Lu and Y) were synthesized. Here, we present the hydrothermal synthesis of the hexagonal late rare-earth manganites $LnMnO_3$ (Ln = Er–Lu and Y) in addition to the orthorhombic $HoMnO_3$ analog in moderate to high yields. Elevated reaction temperatures were used to overcome the low solubility of the late rare-earth trihydroxides and particular emphasis is placed on how temperature mediates the transition of insoluble rare-earth trihydroxides to reactive oxide hydroxides. Additionally, magnetic susceptibility measurements confirmed the phase purity of the hexagonal late rare-earth manganite samples and revealed their interesting magnetic behavior.

Experimental

Materials

The rare-earth sesquioxides Dy_2O_3 (Aldrich, 99.99%), Ho_2O_3 (Aldrich, 99.99%), Er_2O_3 (Aldrich, 99.99%), Tm_2O_3 (Alfa Aesar, 99.99%), Yb_2O_3 (Alfa Aesar, 99.99%), and Lu_2O_3 (Alfa Aesar, 99.99%) in addition to Y_2O_3 (Alfa Aesar 99.99%) were heated to 750 °C to decompose any rare-earth hydroxides and carbonates in the starting materials prior to being used. The Mn_2O_3 (Cerac, 99.99%) was used as received.

Synthesis

Samples of polycrystalline rare-earth manganite were prepared from a direct hydrothermal reaction between the rare-earth and manganese sesquioxides. Stoichiometric amounts (*e.g.*, 0.7160 g of Lu_2O_3 and 0.2840 g Mn_2O_3; 1.0 g total mass; 1.80 mmol of each reagent) of these reagents were weighed and then ground together thoroughly in an agate mortar. For reactions involving Yb_2O_3 or Lu_2O_3, the mixture was then transferred along with 10 mL of a NaOH solution (2.5 M) to a 23 mL poly(tetrafluoroethylene) (PTFE)-lined pressure vessel, which was then sealed. Reactions were run at the appropriate temperature (Table 1) for 48 hours and upon completion of the heating profile, the pressure vessel was allowed to cool naturally to room temperature. The precipitates were then collected by filtration and washed with distilled water several times. After drying in a desiccator for 12 h, the product powders were collected for characterization.

Table 1 $Ln(OH)_3$–LnO(OH) transition temperatures and reaction temperatures that yielded phase-pure $LnMnO_3$

$LnMnO_3$	Transition Temperature (°C)	Reaction Temperature (°C)
$LuMnO_3$	100	175
$YbMnO_3$	140	225
$TmMnO_3$	220	275
$ErMnO_3$	250	300
$HoMnO_3$	300	350
$YMnO_3$	300	350

For reaction temperatures beyond those accessible in PTFE-lined reaction vessels (>250 °C), a 300 mL stainless steel Parr pressure vessel (Series 4760) fitted with a PTFE-flat gasket was used. Stoichiometric amounts (1.5 g total mass) of the constituent oxides, Ln_2O_3 (Ln = Dy, Ho, Er, Tm, and Y) and Mn_2O_3, were weighed and then ground together in an agate mortar. The mixture was then added with 100 mL of NaOH solution (2.5 M) to the 300 mL pressure vessel and heated at the appropriate temperature (Table 1) for 48 hours.

Powder X-ray analysis

Powder X-ray diffraction (PXD) data were recorded on a Scintag XDS 2000 diffractometer with Ni-filtered Cu Kα radiation operating at 40 kV and 20 mA. Data were collected in the 2θ range of 10° to 80° by scanning every 0.02° for 1 s. The PXD pattern of the rare-earth manganite was matched to the appropriate JCPDS file, if available, using the Jade® software suite.[32] Moreover, the experimental powder data were matched to a calculated PXD pattern generated from published crystallographic data by the PowderCell® software suite.[33]

Electron microscope analysis

Electron microscopy studies of certain rare-earth manganites were carried out using a Hitachi S-4500 scanning electron microscope (SEM). To prepare samples, polycrystalline samples were attached to an aluminium mount using carbon tape and coated with 5 nm of gold.

Magnetic measurements

The direct current magnetic susceptibility, both under zero-field cooling (ZFC) and field cooling (FC), of the hexagonal late rare-earth manganites, $LnMnO_3$ (Ln = Er–Lu), was measured over a range of temperatures (5–400K) with a 100 Oe applied field on a superconducting quantum interference device magnetometer (SQUID, Quantum Design, MPMS-5S).

Results and discussion

Sample characterization

Samples of polycrystalline rare-earth manganites, $HoMnO_3$, $ErMnO_3$, $TmMnO_3$, $YbMnO_3$ and $LuMnO_3$, along with $YMnO_3$, were prepared in >80% yields (based on the initial amount of the appropriate Ln_2O_3) from the direct hydrothermal reaction between the appropriate Ln_2O_3 and Mn_2O_3. Fig. 2 shows the PXD patterns of phase-pure samples of all hexagonal late rare-earth manganites, $LnMnO_3$ (Ln = Er–Lu). The inset of Fig. 2 highlights a concomitant shift in the $LnMnO_3$ (110) and (111) reflections (*e.g.*, 2θ = 29.5° and 30.6° for $LuMnO_3$) to a smaller 2θ upon substituting lutetium with progressively larger rare-earth cations. Close inspection of the patterns reveals small shoulders on the (110) and (111) peaks. Since no phases other than the two already described within this manuscript (*i.e.* hexagonal and orthorhombic) have been reported, this observation necessitates further studies to determine their origin. These samples and $YMnO_3$ were indexed with a hexagonal unit cell (space group $P6_3cm$). In contrast, under similar conditions $HoMnO_3$ crystallizes in the orthorhombic (space group *Pnma*) perovskite phase (Fig. 3). Discrepancies between the intensities of certain reflections in the experimental and calculated patterns were observed, but are unexplained at the present time and warrant further attention. Previous studies utilizing soft chemistry techniques (*e.g.*, hydrothermal, citrate method, *etc.*) also yielded the orthorhombic $HoMnO_3$ phase.[34,35] The autogenous pressure (~55 atm at 350 °C) generated during hydrothermal syntheses favors the transition from the hexagonal phase to the denser perovskite phase (*i.e.*, it increases in $HoMnO_3$ from 4.31 standard atomic weight/Å^3 for the hexagonal phase to 4.74 s.a.w./Å^3 for the perovskite phase). The unit cell parameters for each rare-earth manganite are in agreement with previous reports.[36] In addition to PXD, magnetic susceptibility measurements (Fig. 4) confirm the phase purity of the hexagonal rare-earth manganite samples, $LnMnO_3$ (Ln = Er–Lu). The absence of a ferromagnetic transition at ~43K suggests that less than 100 ppm of Mn_3O_4, a common minority phase in solid state preparations, is present in the samples.[37] The SEM image in Fig. 5 illustrates that the particle sizes for rare-earth manganite crystallites, which consist of needles and plates, range from one to a few microns.

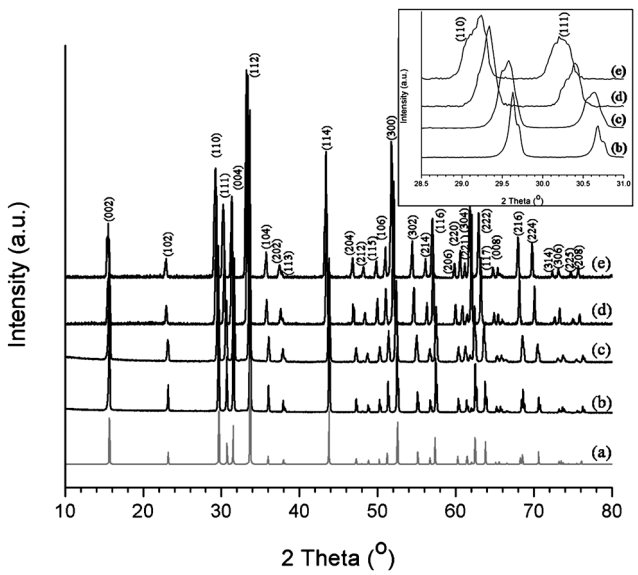

Fig. 2 The PXD patterns of the b) $LuMnO_3$ (JCPDS 14-0030, a = 6.045 Å, c = 11.394 Å), c) $YbMnO_3$ (JCPDS 25-1077, a = 6.059 Å, c = 11.357 Å), d) $TmMnO_3$ (JCPDS 25-1075, a = 6.081 Å, c = 11.376 Å), and e) $ErMnO_3$ (JCPDS 14-0689, a = 6.117 Å, c = 11.435 Å) products are shown in black. The calculated PXD pattern of a) $LuMnO_3$ is shown in gray as a reference. The inset illustrates the shift to smaller 2θ of the (110) and (111) reflections with the increase in ionic radius from Lu^{3+} to Er^{3+}.

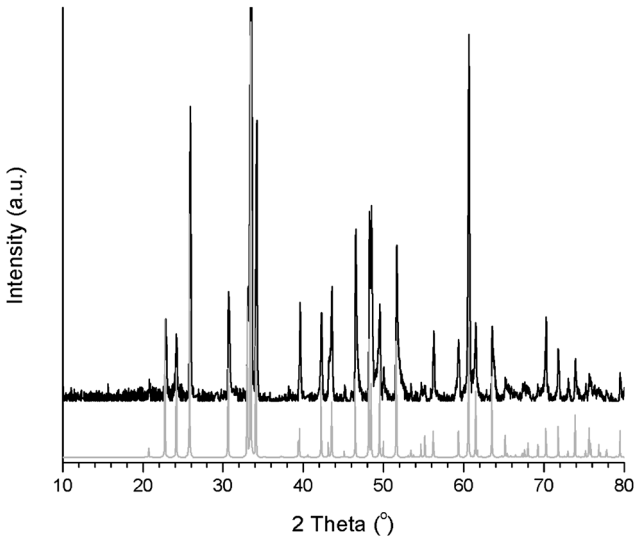

Fig. 3 The PXD pattern of the orthorhombic perovskite $HoMnO_3$ (JCPDS 20-00711, a = 5.260 Å, b = 5.843 Å, c = 7.358 Å, space group *Pnma*). Calculated positions, both indexed and indicating relative intensities, are shown in grey for $HoMnO_3$.

Effects of pH and temperature

The yield of the reaction product is sensitive to pH, temperature, and time, all of which influence the solubility of the rare-earth and manganese cation complexes in aqueous solution. In particular, the pH of the reaction solution, which scales with the addition of a NaOH mineralizer, has a significant effect on the manganese cation solubility. For example, reactions at neutral pH (no NaOH added) yield a mixture of $Ln(OH)_3$/LnO(OH) and Mn_2O_3, indicating that Mn_2O_3 does not dissolve under these conditions. In contrast, at the appropriate temperature, reactions incorporating a NaOH mineralizer generate the desired $LnMnO_3$ product. Mn_2O_3 is an amphoteric oxide that exhibits a minimum solubility in neutral conditions and forms the soluble hydroxomanganite complex, $Mn(OH)_4^-$, at high pH.[38] The solubility of this complex scales with hydroxide concentration and at ambient temperature in a 3M NaOH solution the reported concentration of $Mn(OH)_4^-$ ions is ~10^{-3} mol/L. As with other transition metal cation complexes, the aqueous solubility of $Mn(OH)_4^-$ is expected to increase with rising temperature. Elevated temperatures and the addition of a NaOH mineralizer generated soluble and reactive manganese species.

In contrast to Mn_2O_3, the solubilities of yttrium and rare-earth oxides do not change significantly with an increase in pH at room

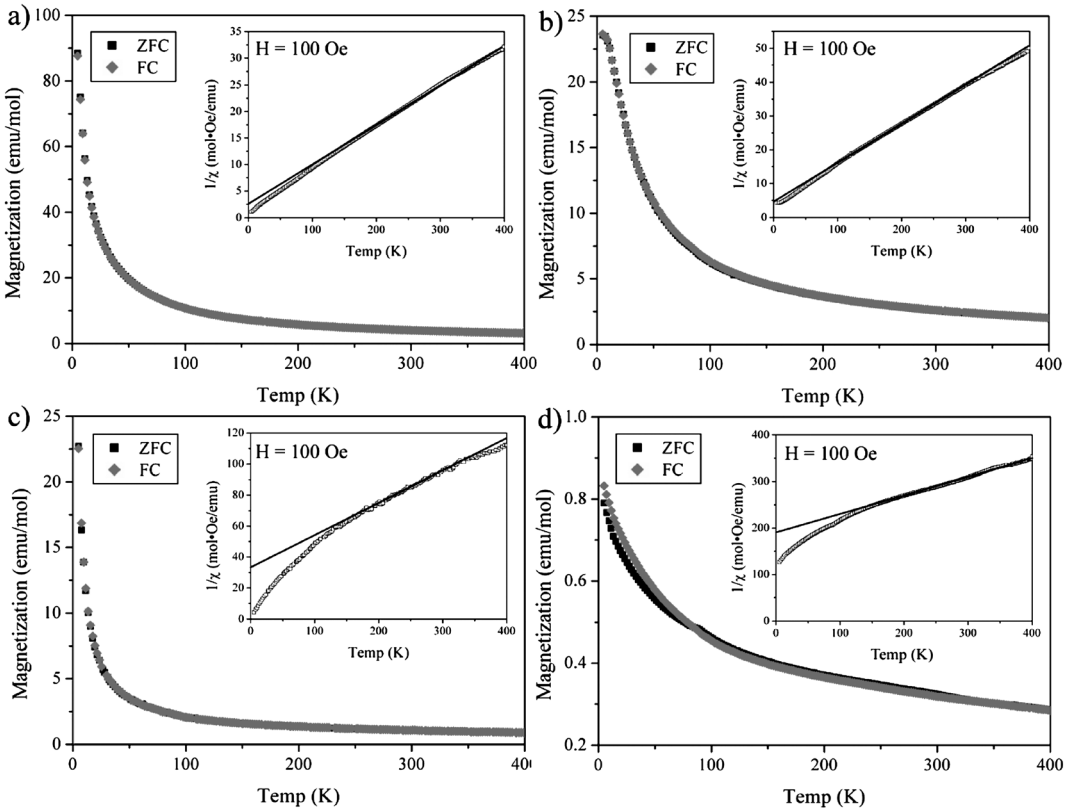

Fig. 4 Zero-field-cooled (ZFC) and field-cooled (FC) magnetization curves of a) $ErMnO_3$, b) $TmMnO_3$, c) $YbMnO_3$, and d) $LuMnO_3$ in an applied field of 100 Oe. The insets plot the reciprocal susceptibilities for the respective $LnMnO_3$ and the linear portions are fit over a variable temperature range.

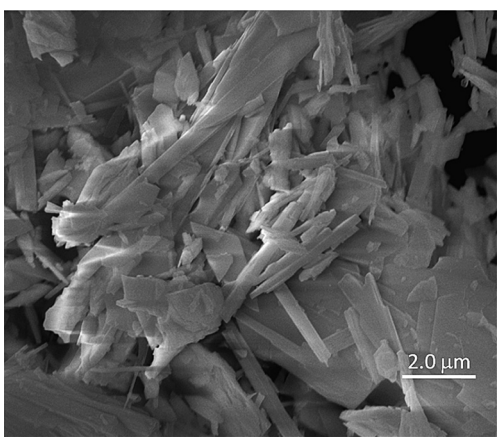

Fig. 5 SEM image of a cluster of $LuMnO_3$ needle- and plate-like crystallites ranging in size from 1–10 μm.

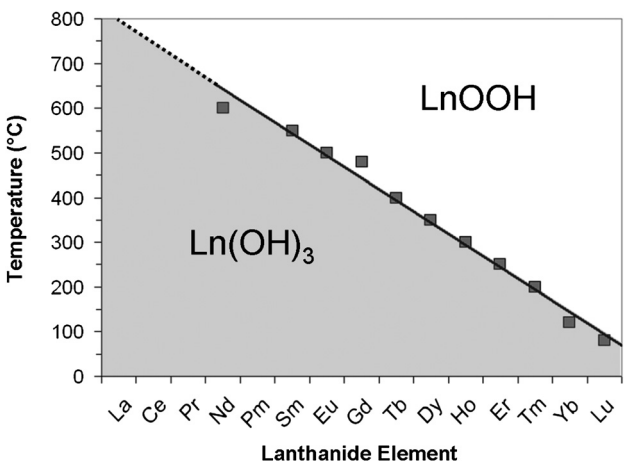

Fig. 6 A graph illustrating the temperature boundary (the line is drawn as a guide to the eye) that separates the stability ranges of rare-earth trihydroxides from the rare-earth oxide hydroxides in hydrothermal conditions. Adapted from Klevtsov.[42]

temperature.[39] Instead, the speciation and reactivity of the rare-earth cation are strongly correlated to the reaction temperature and a minimum temperature threshold, which is dependent on the rare-earth oxide (Fig. 6), must be attained to initiate a reaction. Rare-earth oxides react readily with water to generate stable trihydroxides, $Ln(OH)_3$, and at room temperature the solubility of the rare-earth oxides in aqueous alkaline solutions is negligible.[40] The extent of rare-earth trihydroxide dissolution and formation of an aqueous complex increases at higher temperature, where decreasing values of the dielectric constant for water reduce the shielding of the Ln^{3+} cations from aqueous ligands. Although higher pressures will offset this somewhat, complexation and the increased dissolution at elevated temperature enhance the solubility of rare-earth cations. At the same time, at elevated temperatures the rare-earth trihydroxides dehydrate to the more soluble and reactive rare-earth oxide hydroxide, LnO(OH), with the release of water. As illustrated in Fig. 6, this

transition proceeds at lower temperatures with an increase in atomic number. Such a trend results from the decrease in basicity of the rare-earth trihydroxides when proceeding from lanthanum to lutetium, as would be expected from the decrease in their ionic radius.[41,42] It should be noted that syntheses attempted at temperatures below the dehydration temperature of the respective rare-earth trihydroxide result in no reaction. Therefore, dehydration of the rare earth trihydroxide to the more reactive oxide hydroxide is a necessary step in the hydrothermal synthesis of the late rare-earth manganites.

While a reaction temperature above the transition temperature is a prerequisite for the formation of the desired $LnMnO_3$ product, reactions performed near the transition temperature yield a small amount of $LnMn_2O_5$, a mixed valent (Mn^{3+}/Mn^{4+}) alternate phase. Sufficient oxygen exists in the head space of the pressure vessel to oxidize a small percent of the aqueous Mn^{3+} to Mn^{4+}, and thus account for the formation of $LnMn_2O_5$. To understand the oxidation process, the effect of reaction temperature and time on the product composition of the Yb_2O_3–Mn_2O_3 system, as determined by PXD, was examined and the results are summarized in Table 2. No reaction occurs below the 140 °C threshold, which represents the decomposition temperature of $Yb(OH)_3$. Above the threshold, $Yb(OH)_3$ transitions to YbO(OH) and $YbMnO_3$ begins to form, becoming more abundant with increasing temperature. While a reaction temperature near the transition threshold yields $YbMnO_3$ and a trace amount of $YbMn_2O_5$ over 72 h, a reaction temperature that significantly exceeds the threshold temperature (>220 °C) yields phase-pure $YbMnO_3$ in 24 h. These observations indicate that the formation of $YbMnO_3$ involves the decomposition of the insoluble $Yb(OH)_3$ to the more reactive YbO(OH). Although dehydration of $Yb(OH)_3$ initiates at ~140 °C, the rate of dehydration increases with temperature, accelerating the formation of $YbMnO_3$. Owing to the slow rate of $Yb(OH)_3$ dehydration near the threshold temperature, modest yields are observed only with long reaction times, during which some of the Mn^{3+} oxidizes to Mn^{4+}, resulting in small amounts of the mixed valent $YbMn_2O_5$ phase. Therefore, while a reaction temperature above the threshold temperature is necessary for the formation of $LnMnO_3$, phase-pure samples are prepared only at temperatures sufficiently above the threshold temperature (Table 1). While the phase pure synthesis of $LnMnO_3$ (Ln = Ho–Lu and Y) was possible under the present reaction conditions, owing to the higher decomposition temperature of $Dy(OH)_3$ (~350 °C), attempts to synthesize $DyMnO_3$ yielded a mixture of $DyMnO_3$, $DyMn_2O_5$, DyOOH, and $Dy(OH)_3$. A pressure vessel capable of exceeding 400 °C would be necessary to synthesize phase-pure $DyMnO_3$ and avoid the secondary phase, $DyMn_2O_5$.

Table 2 Reaction products for the reaction between Yb_2O_3 and Mn_2O_3 at certain reaction temperatures and time

Temperature (°C)	Time (h)	Reaction Product[a]
125	24	$Yb(OH)_3$
125	72	$Yb(OH)_3$
150	24	YbO(OH), $Yb(OH)_3$, $YbMnO_3$
150	72	$YbMnO_3$, YbO(OH), $Yb(OH)_3$, $YbMn_2O_5$
180	24	$YbMnO_3$, YbO(OH)
180	72	$YbMnO_3$, YbO(OH), $YbMn_2O_5$
210	24	$YbMnO_3$, YbO(OH)
210	72	$YbMnO_3$, $YbMn_2O_5$
225	24	$YbMnO_3$
250	24	$YbMnO_3$

[a] As determined by PXD. Products are listed from most to least abundant.

The role of head space oxygen in the oxidation of Mn^{3+} and formation of $YbMn_2O_5$ was elucidated by performing experiments in the absence of air. Oxygen was eliminated from both the backfill water and head space of the pressure vessel by using deoxygenated water and sealing the pressure vessel under nitrogen, respectively. Although some oxygen can permeate into the water during the reaction from the Teflon liner, these procedures removed the stoichiometric quantities of oxygen required to oxidize significant amounts of Mn^{3+} to Mn^{4+}. Nonetheless, a reaction between Yb_2O_3 and Mn_2O_3 at 200 °C for 72 h still yielded $YbMn_2O_5$ as a secondary product, albeit a reduced amount. In addition to $YbMn_2O_5$, a small amount of Mn_3O_4, the mixed valent (Mn^{2+}/Mn^{3+}) spinel, was also generated as a second alternate phase in this oxygen-free reaction. The observation of such phases suggests that during the reaction a small percentage of the Mn^{3+} cations disproportionate into Mn^{2+} and Mn^{4+}, generating trace amounts of Mn_3O_4 and $YbMn_2O_5$, respectively. At higher reaction temperatures, the rate of $Yb(OH)_3$ decomposition increases, limiting the time for Mn^{3+} disproportionation, and Mn_3O_4 and $YbMn_2O_5$ are not observed. Whether or not oxygen is present in the autoclave, as seen in Table 1, phase pure $LnMnO_3$ is prepared only at temperatures sufficiently above the decomposition temperature of the respective rare-earth hydroxide.

Magnetic susceptibility measurements

In the hexagonal late rare-earth manganites, antiferromagnetic order of Mn^{3+} ions is established at the Néel temperature (T_N). According to previous studies, the magnetic unit cell coincides with the crystallographic unit cell.[43,44] The magnetic moments of Mn^{3+} are oriented within the *c*-plane and are arranged in a two-dimensional triangular network, where the moments of three neighboring Mn^{3+} ions in the same MnO plane are oriented at angles of 120° with respect to each other.[45,46] The magnetic properties of the hexagonal $LnMnO_3$ (Ln = Er–Lu) samples were studied using zero field cooled (ZFC) and field cooled (FC) magnetic susceptibility (χ) measurements at an applied field of 100 Oe. Spectra collected from 5–400 K (Fig. 4) reveal that the magnetic properties of these phases are dependent on the identity of the rare-earth cation. Changes in the ionic radius of rare-earth cations affect the magnetic properties of $LnMnO_3$ by influencing the Mn–Mn exchange interactions. As shown in Fig. 4, the ZFC curves resemble the FC curves and exhibit only a slight deviation of magnetization below T_N in the $LuMnO_3$ sample (Fig. 4d).

The inverse magnetic susceptibilities ($1/\chi$) are shown in the insets of Fig. 4. The linear portions of these plots were fit and used to obtain the paramagnetic Curie-Weiss temperatures (θ_{CW}) and effective magnetic moments (μ_{eff}). Each curve deviates from the Curie-Weiss law at low temperatures, which is understood in

Table 3 Néel temperature and constants of Curie-Weiss plot of hexagonal $LnMnO_3$

$LnMnO_3$	μ_{eff} (exp)	μ_{eff} (calc)	T_N (K)	θ_{CW}	$\lvert\theta_{CW}\rvert/T_N$
$ErMnO_3$	10.7	10.7	83	−60	0.72
$TmMnO_3$	8.5	9.0	86	−49	0.57
$YbMnO_3$	6.4	6.7	89	−169	1.89
$LuMnO_3$	4.7	4.9	92	−508	5.52

terms of the onset of the magnetic order of Mn^{3+}. The deviation is very slight for $ErMnO_3$ and $TmMnO_3$ because of the large paramagnetic effect of Ln^{3+}. The downward deviation of the curves suggests that the magnetization is increased by spin-canting.[47–49] Values of θ_{CW} and μ_{eff} (exp) along with T_N, calculated effective magnetic moments (μ_{eff}), and frustration parameters ($|\theta_{CW}|/T_N$) are collected in Table 3. Values for T_N were taken as the temperature where the kink in the plot of dM/dT versus T occurs and values for μ_{eff} (exp) and μ_{eff} (calc) were determined as described elsewhere.[31,49,50] The effective magnetic moment of $LnMnO_3$ increases as one proceeds from Ln = Lu to Er, arising from the increased paramagnetic contribution from the rare-earth cation. For each sample, μ_{eff} (exp) and μ_{eff} (calc) are in close agreement, indicating that the magnetization is derived solely from contributions by the Ln^{3+} and Mn^{3+} cations (*i.e.* μ_{eff} of $ErMnO_3$ is very close to that estimated from the free-ion Er^{3+} (9.6 μ_B) and the spin-only Mn^{3+} (4.9 μ_B) moments). In general, the value of $|\theta_{CW}|$ increases with decreasing ionic radius of Ln^{3+}. This is qualitatively consistent with an increase in magnetic interactions originating from the shortening of the *a*-axis, as well as a monotonic decrease in the paramagnetic effect of Ln^{3+}.[49] Values of T_N are all close to those reported previously.[44,51] As with $|\theta_{CW}|$, its monotonic increase with increasing atomic number of Ln is attributed to enhanced antiferromagnetic interactions between Mn^{3+} cations as the *a*-axis shortens. In the case of $YbMnO_3$ and $LuMnO_3$, the absolute values of θ_{CW} are much larger than the ordering temperature, T_N. The ratio between these parameters is a measure of the geometrical frustration of the two-dimensional antiferromagnetic triangular Mn–O lattice.[50] Moderate levels of geometric frustration have been observed previously in polycrystalline samples of both compounds.[45,49,52]

Conclusions

Micrometer-sized crystallites of composition $LnMnO_3$ (Ln = Ho–Lu Y) were prepared on a gram scale by the hydrothermal reaction between the appropriate rare-earth sesquioxide and Mn_2O_3. While alkaline conditions were necessary for the solubilization of manganese, a reaction temperature sufficiently above the decomposition temperature of the respective rare-earth trihydroxide accelerated the rate of transition to the more reactive and soluble rare-earth oxide hydroxide and yielded the $LnMnO_3$ phase. Short reaction times and elevated temperatures limited the oxidation and disproportion of manganese and prevented the formation of alternate phases, Mn_3O_4 and $LnMn_2O_5$. Magnetic susceptibility measurements confirmed the phase purity of the as-prepared polycrystalline $LnMnO_3$ (Ln = Er–Lu) samples and revealed their antiferromagnetic nature.

Acknowledgements

The authors gratefully acknowledge support from the Department of Energy, National Renewable Energy Laboratory Subcontract (Award No. XAT-5-33636-02/DE-AC36-98GO) and Basic Energy Sciences (Award No. DE-FG02-06ER46320 and Award No. DE-FG02-08ER46536). The authors made use of Central Facilities supported by the MRSEC program of the National Science Foundation (Grant DMR-0520513) at the Materials Research Center of Northwestern University. This work was partially carried out in the frame of the STREP MaCoMuFi (NMP3-CT-2006-033221) supported by the European Community and by the CNRS France. The SEM work was performed by M. Russell and S. DiBenedetto in the EPIC facility of NUANCE Center at Northwestern University. NUANCE Center is supported by NSF-NSEC, NSF-MRSEC, Keck Foundation, the State of Illinois, and Northwestern University. W.C.S was additionally supported through a Natural Science and Engineering Research Council of Canada (NSERC) Postgraduate Doctoral Scholarship, Chateaubriand Post-doctoral Fellowship, and the Conseil Régional de Basse-Normandie (CRBN).

References

1 G. H. Jonker and J. H. van Santen, *Physica*, 1950, **16**, 599–600.
2 E. F. Bertaut, F. Forrat and P.-H. Fang, *Compt. Rend.*, 1963, **256**, 1958–1961.
3 E. F. Bertaut, R. Pauthenet and M. Mercier, *Phys. Lett.*, 1963, **7**, 110–111.
4 C. N. R. Rao and A. K. Cheetham, *Science (Washington, D.C.)*, 1996, **272**, 369–370.
5 A. P. Ramirez, *J. Phys.: Condens. Matter*, 1997, **9**, 8171–8199.
6 M. Fiebig, T. Lottermoser, D. Frohlich, A. V. Goltsev and R. V. Pisarev, *Nature (London, United Kingdom)*, 2002, **419**, 818–820.
7 A. Filippetti and N. A. Hill, *Phys. Rev. B: Condens. Matter*, 2002, **65**, 195120.
8 C. Ederer and N. A. Spaldin, *Nat. Mater.*, 2004, **3**, 849–851.
9 N. A. Spaldin and M. Fiebig, *Science (Washington, DC, United States)*, 2005, **309**, 391–392.
10 C. N. R. Rao and C. R. Serrao, *J. Mater. Chem.*, 2007, **17**, 4931–4938.
11 K. Yamauchi, F. Freimuth, S. Blugel and S. Picozzi, *Phys. Rev. B*, 2008, **78**, 014403.
12 M. T. Anderson, K. B. Greenwood, G. A. Taylor and K. R. Poeppelmeier, *Prog. Solid State Chem.*, 1993, **22**, 197–233.
13 I. Naray-Szabo, *Naturwissenschaften*, 1943, **31**, 466.
14 R. C. Vickery and A. Klann, *J. Chem. Phys.*, 1957, **27**, 1161–1163.
15 K. P. Belov, M. A. Zaitseva and A. V. Ped'ko, *Zh. Eksp. Teor. Fiz.*, 1959, **36**, 1672–1679.
16 B. B. Van Aken, A. Meetsma and T. T. M. Palstra, *Acta Crystallogr., Sect. C*, 2001, **C57**, 230–232.
17 F. S. Galasso, *Structure, Properties, and Preparation of Perovskite-Type Compounds (International Series of Monographs in Solid State Physics, Vol. 5)*, Pergamon Press, New York, 1969.
18 P. A. Salvador, T.-D. Doan, B. Mercey and B. Raveau, *Chem. Mater.*, 1998, **10**, 2592–2595.
19 O. Carp, L. Patron, A. Ianculescu, J. Pasuk and R. Olar, *J. Alloys Compd.*, 2003, **351**, 314–318.
20 A. Waintal and J. Chenavas, *Mater. Res. Bull.*, 1967, **2**, 819.
21 C. N. R. Rao; B. Raveau, Editors, *Colossal Magnetoresistance, Charge Ordering, and Related Properties of Manganese Oxides*, World Scientific, New Jersey, 1998.
22 H. L. Yakel Jr., W. C. Koehler, E. F. Bertaut and F. Forrat, *Acta Cryst.*, 1963, **16**, 957–962.
23 J. S. Zhou, J. B. Goodenough, J. M. Gallardo-Amores, E. Moran, M. A. Alario-Franco and R. Caudillo, *Phys. Rev. B*, 2006, **74**, 014422.

24 Z. J. Huang, Y. Cao, Y. Y. Sun, Y. Y. Xue and C. W. Chu, *Phys. Rev. B: Condens Matter*, 1997, **56**, 2623–2626.
25 J. E. Medvedeva, V. I. Anisimov, M. A. Korotin, O. N. Mryasov and A. J. Freeman, *J. Phys.: Condens. Matter*, 2000, **12**, 4947–4958.
26 P. A. Sharma, J. S. Ahn, N. Hur, S. Park, B. Kim Sung, S. Lee, J. G. Park, S. Guha and S. W. Cheong, *Phys.Rev. Lett.*, 2004, **93**(93), 177202.
27 A. B. Souchkov, J. R. Simpson, M. Quijada, H. Ishibashi, N. Hur, J. S. Ahn, S. W. Cheong, A. J. Millis and H. D. Drew, *Phys. Rev. Lett.*, 2003, **91**, 027203.
28 B. B. Van Aken and T. T. M. Palstra, *Phys. Rev. B: Condens. Matter*, 2004, **69**, 134113.
29 N. Mufti, A. A. Nugroho, G. R. Blake and T. T. M. Palstra, *Phys. Rev. B: Condens. Matter*, 2008, **78**, 024109.
30 Y. Chen, H. Yuan, G. Tian, G. Zhang and S. Feng, *J. Solid State Chem.*, 2007, **180**, 1340–1346.
31 Y. Chen, H. Yuan, G. Li, G. Tian and S. Feng, *J. Cryst. Growth*, 2007, **305**, 242–248.
32 *Jade, 5.0*; Materials Data Inc.: Livermore, CA,1999.
33 *PowderCell, 2.4*; Federal Institute for Materials Research and Testing: Berlin, Germany, 2000.
34 Y. Wang, X. Lu, Y. Chen, F. Chi, S. Feng and X. Liu, *J. Solid State Chem.*, 2005, **178**, 1317–1320.
35 J. A. Alonso, M. T. Casais, M. J. Martinez-Lope and I. Rasines, *J. Solid State Chem.*, 1997, **129**, 105–112.
36 J. S. Zhou, J. B. Goodenough, J. M. Gallardo-Amores, E. Moran, M. A. Alario-Franco and R. Caudillo, *Phys. Rev. B: Condens. Matter*, 2006, **74**, 014422.
37 D. G. Tomuta, S. Ramakrishnan, G. J. Nieuwenhuys and J. A. Mydosh, *J. Phys.: Condens. Matter*, 2001, **13**, 4543–4552.
38 F. Chouaib, P. H. Heubel, M. Del Carmen Sanson, G. Picard and B. Tremillon, *J. Electroanal. Chem. Interfacial Electrochem.*, 1981, **127**, 179–193.
39 P. V. Klevtsov and L. P. Sheina, *Neorg. Mater.*, 1965, **1**, 912–917.
40 S. Deberdt, S. Castet, J.-L. Dandurand, J.-C. Harrichoury and I. Louiset, *Chem. Geol.*, 1998, **151**, 349–372.
41 M. N. Viswanathiah, J. A. K. Tareen and T. R. N. Kutty, *Mater. Res. Bull.*, 1980, **15**, 855–859.
42 P. V. Klevtsov and L. P. Sheina, *Izv. Akad. Nauk, Neorg. Mater.*, 1965, **1**, 912–917.
43 M. Fiebig, D. Frohlich, K. Kohn, S. Leute, T. Lottermoser, V. V. Pavlov and R. V. Pisarev, *Phys. Rev. Lett.*, 2000, **84**, 5620–5623.
44 W. C. Koehler, H. L. Yakel Jr., E. O. Wollan and J. W. Cable, *Phys. Lett.*, 1964, **9**, 93–95.
45 S. Lee, M. Kang, C. Lee, A. Hoshikawa, M. Yonemura, T. Kamiyama and J. G. Park, *Physica B*, 2006, **385–386**, 405–407.
46 H. Sugie, N. Iwata and K. Kohn, *J. Phys. Soc. Jpn.*, 2002, **71**, 1558–1564.
47 M. Bieringer and J. E. Greedan, *J. Solid State Chem.*, 1999, **143**, 132–139.
48 A. Munoz, J. A. Alonso, M. J. Martinez-Lope, M. T. Casais, J. L. Martinez and M. T. Fernandez-Diaz, *Phys. Rev. B: Condens. Matter*, 2000, **62**, 9498–9510.
49 K. Yoshii and H. Abe, *J. Solid State Chem.*, 2002, **165**, 131–135.
50 K. H. J. Buschow, Editor, *Handbook of Magnetic Materials, Vol. 13;* Elsevier: New York, 2001.
51 T. Katsufuji, S. Mori, M. Masaki, Y. Moritomo, N. Yamamoto and H. Takagi, *Phys. Rev. B: Condens. Matter*, 2001, **64**, 104419.
52 D. G. Tomuta, S. Ramakrishnan, G. J. Nieuwenhuys and J. A. Mydosh, *J. Phys.: Condens. Matter*, 2001, **13**, 4543–4552.